

Tuning the Nucleophilicity of Anion in Lithium Salt to Enable an Anion-Rich Solvation Sheath for Stable Lithium Metal Batteries

Pan Zhou, Yu Ou, Qingqing Feng, Yingchun Xia, Haiyu Zhou, Wen-hui Hou, Xuan Song, Yang Lu, Shuaishuai Yan, Weili Zhang, Yun He, and Kai Liu*

Traditional lithium salts typically adhere to the designing principles of enhancing cation-anion dissociation degree to obtain a high electrolyte conductivity. This promotes the invention of lithium bis(trifluoromethanesulfonyl)imide (LiTFSI), where the symmetric electron-withdrawing trifluoromethanesulfonyl groups significantly delocalize the negative charge density around the nitrogen atom, thereby weakening the electrostatic interaction between Li^+ and the anion. Herein, deviating from the general principle, lithium (methanesulfonyl)(trifluoromethanesulfonyl) imide (LiMTFSI) is deliberately designed by substituting a unilateral electron-withdrawing trifluoromethyl ($-\text{CF}_3$) group of LiTFSI with an electron-donating methyl ($-\text{CH}_3$) group, to tune the nucleophilicity of the anion. This modification enhances Li-anion interaction, causing the anion to replace the solvent molecules in the Li^+ solvation shell. Additionally, the MTFSI $^-$ anion exhibits an elevated donor number to facilitate the solubility of LiNO_3 in carbonate-based electrolytes. The synergistic effect of these changes suppresses the decomposition of solvent and helps construct a stable solid electrolyte interphase (SEI) enriched with multiple inorganic lithium salts (e.g., Li_2S , Li_3N , and LiN_xO_y) on the Li metal anode, which enables the 500 mAh $\text{Li}||\text{LiNi}_{0.5}\text{Co}_{0.2}\text{Mn}_{0.3}\text{O}_2$ pouch cell to operate steadily for 150 cycles. It is believed this work would provide new insights and another dimension for designing functional anions beyond their role as charge carriers.

1. Introduction

The pursuit for higher energy density positioned lithium metal batteries (LMB) as one of the most promising candidates for next-generation battery systems, owing to the high specific capacity (3860 mAh g^{-1} , over ten times that of graphite) and low electrochemical reduction potential (-3.04 V vs standard hydrogen electrode, $\approx 0.1 \text{ V}$ lower than the graphite) of Li metal anode.^[1] Among all the components of LMB, the electrolyte plays a pivotal role in dictating the electrochemical performances by influencing both the bulk electrolyte properties and interfacial behavior.^[2] Thus, tuning the electrolyte chemistry is essential for achieving stable LMB operation.

In conventional electrolyte formulations, solvents with high dielectric constant (e.g., ethylene carbonate (EC)) and lithium salts with high dissociation degree (e.g., lithium hexafluorophosphate (LiPF_6) and lithium bis(trifluoromethanesulfonyl)imide (LiTFSI)) are chosen to ensure high conductivity.^[2a,b] Consequently, Li^+ ions and anions are well separated, and Li^+ ions typically coordinate with several carbonate solvent molecules. These solvent

molecules tend to migrate with Li^+ and decompose on the Li anode, forming a carbonate-derived solid electrolyte interphase (SEI) composed of alkyl lithium carbonate (ROCO_2Li) and oligomers.^[2c,3] However, such an organics-rich SEI cannot adapt to the high-volume change of Li metal during continuous plating/stripping and fails to withstand the high stress produced by lithium dendrites.^[4] In this context, it is widely accepted that shifting from a solvent-derived SEI to an anion-derived SEI benefits the deposition of Li metal,^[5] given that anions tend to be decomposed to form inorganics species (e.g., LiF , Li_2O , and Li_3N), which possess higher chemical stability, mechanical strength, and lower Li^+ diffusion barrier.^[6] Therefore, the use of Li metal anode places higher demand on the function of anions beyond serving as charge carriers. To this end, there are two main strategies to construct an anion-rich Li^+ solvation sheath. The first is to use high-concentration or localized high-concentration electrolytes by increasing the ratio of anions and reducing the ratio

P. Zhou, Y. Ou, Y. Xia, H. Zhou, W.-hui Hou, X. Song, Y. Lu, S. Yan, K. Liu
The State Key Laboratory of Chemical Engineering
Department of Chemical Engineering
Tsinghua University
Beijing 100084, China
E-mail: liukai2019@tsinghua.edu.cn

Q. Feng, W. Zhang
Hefei Institute for Public Safety Research
Tsinghua University
Hefei 230601, China
Y. He
Yew Chung International School of Beijing
Beijing 100018, China

The ORCID identification number(s) for the author(s) of this article can be found under <https://doi.org/10.1002/adfm.202416800>

DOI: 10.1002/adfm.202416800

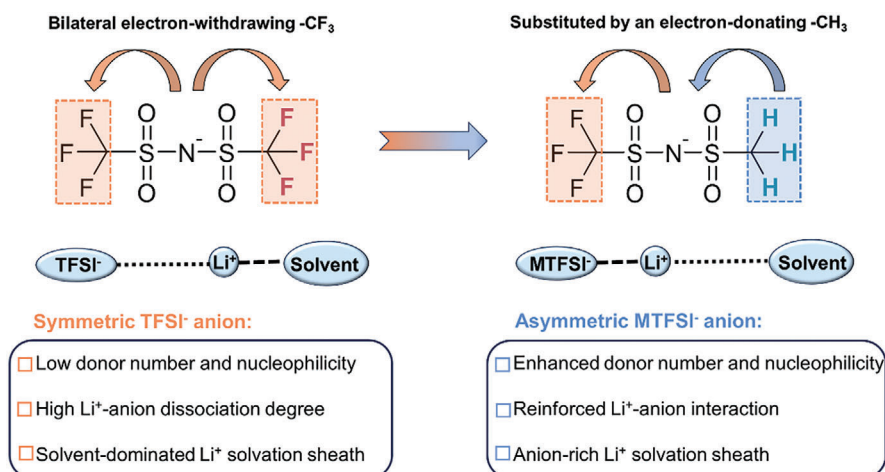


Figure 1. Designing principles of LiMTFSI based on LiTFSI.

of solvent molecules.^[5a,7] The other involves developing weak-solvating solvents, such as fluorinated solvents, to minimize the Li^+ -solvent interaction.^[8] However, the above strategies generally have to increase the viscosity while decreasing the wettability of the electrolytes, etc. In addition, their application is also hindered by economic considerations.

Herein, we propose a third approach to increase anions' participation in the Li^+ solvation sheath without elevating salt concentration or altering solvent type. In this study, a new lithium salt, lithium (methanesulfonyl)(trifluoromethanesulfonyl) imide (LiMTFSI) was devised to regulate the Li^+ solvation shell in carbonate electrolyte and modify the SEI (Figures S1 and S2, Supporting Information). Unlike the conventional rule for designing lithium salts (e.g., LiPF_6 and LiTFSI), which delocalize the negative charge on the anionic center with electron-withdrawing groups to enhance the cation-anion separation degree, LiMTFSI was deliberately designed to reinforce the interaction between Li^+ and MTFSI^- . Based on LiTFSI, a unilateral electron-withdrawing $-\text{CF}_3$ group was substituted by an electron-donating $-\text{CH}_3$ to appropriately enhance the basicity and nucleophilicity of the anion. This substitution strengthens the interaction between MTFSI^- and Li^+ ions, causing more anions to compete with solvent molecules to enter the Li^+ solvation shell and form a sulfur-containing (e.g., Li_2S , Li_2SO_4 , and Li_2SO_3) SEI. Moreover, the rationally tuned donor number (DN) of MTFSI^- anion enables it to exhibit a solubilization effect for LiNO_3 in carbonate electrolyte, which benefits uniform Li deposition by forming a nitride-rich (Li_3N , LiN_xO_y) SEI.^[6a,9] The synergistic effect facilitates the formation of SEI comprised of multiple inorganic lithium salts, which possess lower resistance and help induce smooth Li deposition. As a result, the Coulombic efficiency (CE) for the Li plating/stripping process reaches as high as 98.9% with the LiMTFSI-based carbonate electrolyte. Moreover, this electrolyte enables a practical 500 mAh $\text{Li}||\text{LiNi}_{0.5}\text{Co}_{0.2}\text{Mn}_{0.3}\text{O}_2$ (NCM523) pouch cell to run for 150 cycles with a capacity retention of 87.3%.

2. Results and Discussion

As illustrated in Figure 1, LiMTFSI was designed with two primary considerations: i) The traditional TFSI^- anion is unfav-

orable for ion pairing at a common concentration (e.g., 1 M). In this context, a unilateral electron-withdrawing $-\text{CF}_3$ group is substituted with an electron-donating $-\text{CH}_3$ to appropriately enhance the basicity and nucleophilicity of the anions; ii) the other $-\text{CF}_3$ group is retained to ensure moderate conductivity and provide a fluorine source. Electrostatic potential (ESP) maps reveal that compared to the TFSI^- anion, the MTFSI^- anion exhibits a higher negative electron density around the nitrogen center, especially the region near the methyl (Figure 2a,b). Moreover, theoretical calculations demonstrate that the binding energy for LiMTFSI (-6.543 eV) is significantly more negative than that for traditional LiPF_6 (-5.877 eV) and LiTFSI (-6.106 eV) (Figure 2c). These results indicate that the anion alteration successfully enhances the affinity between Li^+ and anion. However, LiMTFSI can still exhibit a high solubility of ≈ 4.5 M in commercial carbonate solvent (Figure S3, Supporting Information).

The difference in the binding energy of lithium salt then influences the Li^+ solvation environment in the electrolyte. As revealed by ^7Li nuclear magnetic resonance (NMR) spectra, the Li nuclei exhibit a similar chemical shift in LiPF_6 - and LiTFSI-based carbonate electrolytes at the concentration of 1 M (Figure 2d). For these two traditional lithium salts with high dissociation degrees, Li^+ ions are less influenced by anions and more coordinated with solvent molecules, resulting in a similar Li solvation sheath for both electrolytes. However, a broader peak and upfield shift of ^7Li spectra are observed for LiMTFSI electrolyte at the same concentration, with the chemical shift moving from -0.242 ppm for LiTFSI to -0.364 ppm for LiMTFSI. These results indicate that the locally reinforced electron cloud density of the MTFSI^- anion enables it to compete with solvent molecules to bind Li^+ ions. These findings are further supported by Raman spectra (Figure S4, Supporting Information; Figure 2e). Compared with LiPF_6 - and LiTFSI-based electrolytes, a smaller percentage of solvated solvent molecules is observed in the LiMTFSI-based electrolyte. Specifically, 33.2% and 31.4% of EC are in a coordinated state for LiPF_6 and LiTFSI, respectively, while this value drops to 23.8% for LiMTFSI (Figure 2f). Therefore, it can be concluded that LiMTFSI effectively excludes solvent molecules from the Li^+ solvation shell.

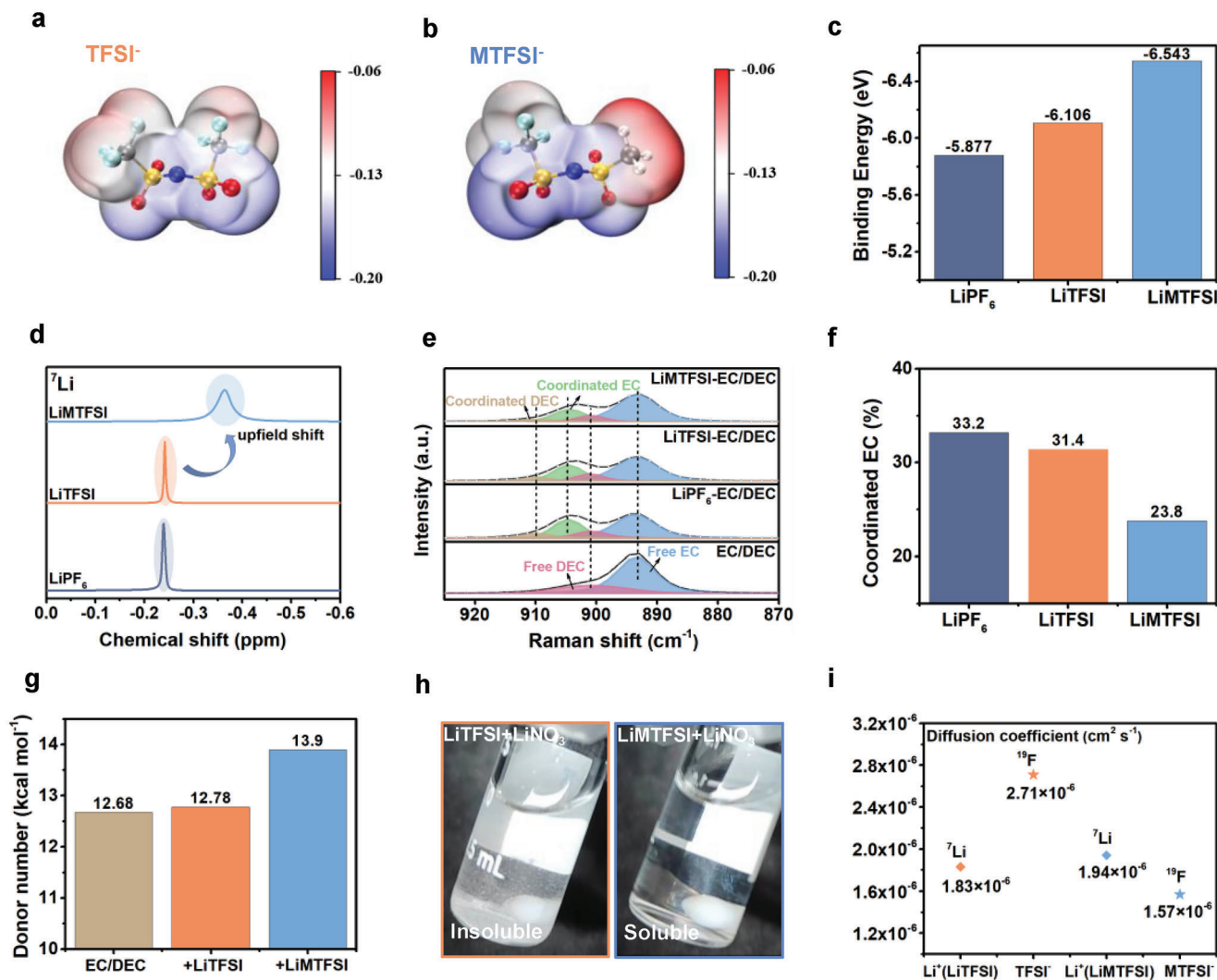


Figure 2. Electrostatic potential maps of a) TFSI⁻ anion and b) MTFSI⁻ anion. c) Binding energy between PF₆⁻, TFSI⁻ and MTFSI anions and Li⁺. d) ⁷Li spectra of EC/DEC-based electrolyte with 1 M LiPF₆, LiTFSI and LiMTFSI, respectively. e) Raman spectra of pure EC/DEC and EC/DEC-based electrolytes with 1 M LiPF₆, LiTFSI and LiMTFSI, respectively. f) The ratio of coordinated EC in EC/DEC-based electrolyte with 1 M LiPF₆, LiTFSI, and LiMTFSI, respectively. g) Determined DN value of pure EC/DEC and EC/DEC-based electrolytes with 1 M LiTFSI and LiMTFSI, respectively. h) The solubility of 0.1 M LiNO₃ in EC/DEC solvent in the presence of 0.1 M LiTFSI (left) and LiMTFSI (right). i) The diffusion coefficient of Li⁺ and anions of LiTFSI and LiMTFSI in EC/DEC solvent.

The electron-donating abilities of TFSI⁻ and MTFSI⁻ were further compared by measuring the donor number (DN) (Figure S5, Supporting Information; Figure 2g).^[10] The donor number, which was first proposed by Gutmann, describes the basicity of solvents or anions.^[10b,11] A higher DN typically indicates a higher possibility of binding with a Lewis acid, which corresponds to Li⁺ in the electrolyte. The DN of EC/DEC (1:1 by vol) was determined to be 12.68 kcal mol⁻¹, with only a subtle change observed when LiTFSI was added (12.78 kcal mol⁻¹) at a concentration of 1 M, which indicates that TFSI⁻ anion is a weak electron donor. However, when LiMTFSI is introduced to the electrolytes instead of LiTFSI, the determined DN value of the electrolyte increases to 13.90 kcal mol⁻¹, indicating that the MTFSI⁻ anion possesses higher nucleophilicity and interacts more strongly with Li⁺. The enhanced DN of MTFSI anion brings an additional

advantage of enhancing the solubility of LiNO₃, an effective additive for uniform Li deposition in carbonate-based electrolytes. Normally, LiNO₃ is hardly dissolved in conventional carbonate electrolytes due to the high binding strength between Li⁺ and NO₃⁻. As shown in Figure 2h, 0.1 M LiNO₃ cannot be dissolved in EC/DEC (1:1 by vol) in the presence of 0.1 M LiTFSI. However, with the assistance of 0.1 M LiMTFSI, 0.1 M LiNO₃ is completely dissolved in the electrolyte. The dual function of excluding solvent molecules from the Li⁺ solvation shell and solubilizing LiNO₃ makes LiMTFSI a promising lithium salt for use in lithium metal batteries.

The differences in interactions among Li⁺, anions, and solvents in turn influence the physicochemical properties of electrolytes, including conductivity and Li⁺ transference number (T₊). As expected, the LiMTFSI-based electrolyte exhibits lower

conductivity than the LiTFSI-based electrolyte (Figure S6, Supporting Information, 0.21 vs 0.43 mS cm⁻¹). However, the Li⁺ transference number (T_+) increases from 0.2 to 0.44 when LiTFSI is replaced by LiMTFSI (Figures S7–S9, Supporting Information). This could be explained by the following considerations: with conventional lithium salts of high dissociation degree, Li⁺ ions are well solvated by the bulky solvent molecules, resulting in a significant decrease in Li⁺ mobility and thus a low T_+ . When an electron-withdrawing –CF₃ group is replaced with –CH₃ group, however, the MTFSI⁻ anion is more prone to compete with the solvent to bind with Li⁺ due to the enhanced nucleophilicity of the anion. The diffusion coefficient determined by diffusion-ordered spectroscopy (DOSY) further reveals the difference. As shown in Figure 2i, the Li⁺ diffusion coefficient in LiMTFSI-based electrolyte (1.94×10^{-6} cm² s⁻¹) is even slightly higher than that in LiTFSI-based electrolyte (1.83×10^{-6} cm² s⁻¹), despite the latter has a higher conductivity. Interestingly, the anion demonstrates an opposite trend. Compared with TFSI⁻ (2.71×10^{-6} cm² s⁻¹), MTFSI⁻ exhibits a lower diffusion coefficient (1.57×10^{-6} cm² s⁻¹) even though the –CH₃ group has a smaller size than the –CF₃ group. These results further validate that, compared with the TFSI⁻ anion, which exists in a “freer” state in the electrolyte, the MTFSI⁻ has a higher tendency to interact with Li⁺ and therefore its migration is constrained, which explains the reason for the increased T_+ . Moreover, when LiMTFSI is introduced to the commercial carbonate electrolyte as an additive at a molar concentration of 0.1 M, it does not negatively affect the overall conductivity and oxidation ability (Figures S10 and S11, Supporting Information).

To fully utilize the beneficial function of LiMTFSI discussed above, 0.1 M LiMTFSI and 0.1 M LiNO₃ were added to the baseline electrolyte (1 M LiPF₆ EC/DEC (1:1 by vol) with 10% vol FEC), forming the LiMTFSI electrolyte. Molecular dynamic (MD) simulations for the baseline and LiMTFSI electrolytes were first conducted to investigate the Li⁺ solvation structure from a more microscopic and quantitative aspect. As shown in Figure S12 (Supporting Information), the radical distribution function of Li⁺ indicates that MTFSI⁻ and NO₃⁻ have a significantly higher possibility to enter into the Li⁺ solvation structure compared to other components, which helps to exclude the solvent molecules and construct an anion-rich solvation shell. Specifically, the average coordination numbers of DEC and EC with Li⁺ are 1.570 and 2.612, respectively, in the baseline electrolyte. These values decrease to 1.461 and 2.287, respectively, with the introduction of LiMTFSI and LiNO₃ (Figures S13 and S14, Supporting Information). Furthermore, we conducted a statistical analysis of the percentage of solvent-separated ion pair (SSIP), contact ion pair (CIP), and aggregate (AGG) in the electrolytes. Notably, the fraction of AGG increases from 24.1% in the baseline electrolyte to 34.6% in the LiMTFSI electrolyte (Figure S15, Supporting Information), indicating a Li⁺ solvation structure enriched with more anions.

Then, the Coulombic efficiency (CE) of the Li deposition/stripping process with the two electrolytes was evaluated in Li||Cu cells using Aurbach's method.^[12] As shown in Figure 3a, the cell with LiMTFSI electrolyte exhibits a higher CE of 98.9% compared to 96.9% with the baseline electrolyte. According to the time–voltage profile, the cell with LiMTFSI electrolyte demonstrates lower voltage hysteresis during the ini-

tial nucleation stage (Figure S16, Supporting Information). During subsequent cycling, the cell with LiMTFSI electrolyte maintains a more stable time–voltage profile and lower overpotential (10.2 mV) compared to the baseline electrolyte (16.0 mV) (Figure 3b). The Tafel curve test provides a more direct comparison of Li deposition kinetics with the two different electrolytes (Figure 3c). According to the fitting results from the Tafel curve (Figure 3d), the LiMTFSI electrolyte significantly enhances the exchange current density (0.808 mA cm⁻²) compared to the baseline electrolyte (0.457 mA cm⁻²), indicating accelerated dynamics for Li deposition. Electrochemical impedance spectroscopy was further conducted to reveal the differences in interfacial resistance. As shown in Figure 3e, the Li||Li cell with LiMTFSI exhibits lower interfacial resistance across various temperatures. For example, the charge transfer resistance (R_{ct}) decreases from 15.4 Ω with the baseline electrolyte to 6.2 Ω with the LiMTFSI electrolyte at 25 °C (Figure 3f), and the activation energy for the charge transfer process declines from 57.9 to 52.4 kJ mol⁻¹ (Figure 3g), demonstrating a reduced energy barrier for the Li⁺ desolvation process. As previously demonstrated, the introduction of LiMTFSI and LiNO₃ effectively excludes the solvent molecules from the Li⁺ solvation structure. Consequently, fewer solvent molecules coordinate with Li⁺, facilitating the desolvation process. Moreover, compared with solvent molecules, negatively charged anions tend to be repelled by the electric field near the Li metal anode.^[13] Therefore, the anion-rich solvation environment reduces the energy barrier for the Li⁺ desolvation process.

The morphology of deposited Li metal was observed by scanning electron microscope (SEM). As shown in Figure 4a, more lithium whiskers appear with baseline electrolyte at a current density of 0.5 mA cm⁻², and this phenomenon intensifies when the current density is increased to 2 mA cm⁻² (Figure S17, Supporting Information). On the contrary, a more compact and smooth morphology of deposited Li metal is observed with the LiMTFSI electrolyte (Figure 4b; Figure S17, Supporting Information). Considering that the interfacial behavior is closely related to the properties of SEI, X-ray photoelectron spectroscopy (XPS) was conducted to investigate the SEI species derived from different electrolytes. The C 1s spectra show that the content of C-containing species including C–O at ≈286.8 eV and R–O–C=O at ≈288.7 eV, which mainly derives from the reduction decomposition of carbonate solvents, decreases in the LiMTFSI electrolyte compared to that in the baseline electrolyte (Figure 4c,d). According to the N 1s spectra (Figure 4e), Li₃N and LiN_xO_y are observed in the SEI formed in the LiMTFSI electrolyte, which can be attributed to the reduction of LiNO₃. Moreover, considering that LiMTFSI is the sole sulfur source in the electrolyte system, the detected signal from the S 2p spectra indicates that LiMTFSI also participates in SEI formation, leading to the formation of sulfate and Li₂S in the SEI (Figure 4f), which are believed to protect the interphase from continuous decomposition.^[14] Therefore, it can be concluded that, compared to the organics-dominant SEI formed in the baseline electrolyte, the introduction of LiMTFSI and LiNO₃ helps to form an anion-rich Li⁺ solvation sheath and suppresses the decomposition of solvent molecules. This synergistic effect aids in constructing an inorganics-rich SEI containing Li₂S, Li₃N, etc. (Figure 4g).

The SEI structure and species were further investigated by time-of-flight secondary ion mass spectrometry (TOF-SIMS),

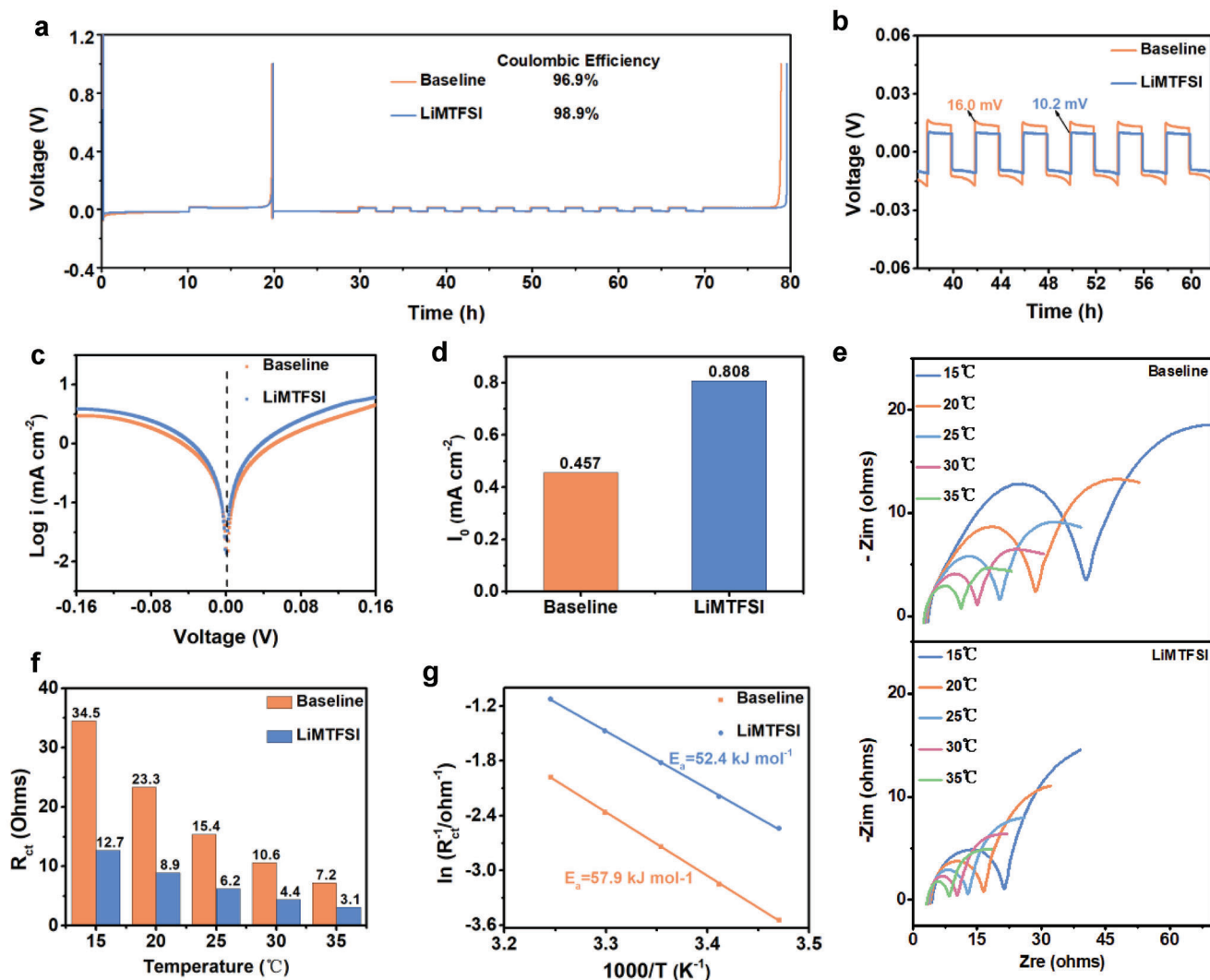


Figure 3. a) Coulombic efficiency of Li plating/stripping process in Li||Cu cells with baseline and LiMTFSI electrolytes. b) Enlarged time–voltage profile of Li||Cu cells. c) Tafel curves of Li||Li cells with baseline and LiMTFSI electrolytes. d) Exchange current density obtained by fitting the Tafel curves. e) Nyquist plots and f) fitted resistance of charge transfer in Li||Li cells with the BE and LiMTFSI electrolytes at various temperatures. g) Arrhenius behavior of the charge transfer resistance for Li⁺ with baseline and LiMTFSI electrolytes.

which vividly presents the spatial distribution of SEI components. The $C_2H_3O^-$ and CHO_2^- species were selected as typical fragments of the organic species in the SEI. According to the top-view images of the TOF-SIMS sputtered volumes of SEI, the content of $C_2H_3O^-$ and CHO_2^- is more enriched in the baseline electrolyte compared to the LiMTFSI electrolyte (Figure 5a–d). This indicates a more aggressive decomposition of the carbonate solvent in the baseline electrolyte. Moreover, depth profile analysis shows that the organic species are distributed across the entire investigated depth of the SEI in the baseline electrolyte. In contrast, the $C_2H_3O^-$ and CHO_2^- species are more evenly distributed on the surface of the SEI in the LiMTFSI electrolyte (Figure 5b,d), indicating a thinner and more uniform SEI structure. The contrast is similarly observed for the CO_3^- species between the two electrolytes (Figure 5e,f), further demonstrating the alleviation of carbonate decomposition in the LiMTFSI electrolyte. The LiF_2^- fragments exhibit a similar distribution pattern in that the de-

composition products are more concentrated on the surface, indicating a thin SEI (Figure S18, Supporting Information). Additionally, the SO_2^- and S^- species are detected on the SEI surface (Figure S19, Supporting Information), validating the reduction of LiMTFSI.

Thus, the mechanism for SEI regulation can be summarized from the following two aspects: i) the rationally tuned nucleophilicity of MTFSI⁻ anion enables it to preferably appear in the Li⁺ solvation shell, thereby excluding more solvent molecules from the solvation shell. This not only helps to mitigate the decomposition of solvent molecules but also facilitates the Li⁺ desolvation process during Li plating, as evidenced by the reduced value of R_{ct} and activation energy of charge transfer. ii) The MTFSI⁻ and NO_3^- anions in the Li⁺ solvation sheath migrate with Li⁺ to the anode surface, where they are reduced to form an inorganics-rich SEI composed of Li_2S , Li_3N , etc. Compared to the fragile and unstable organics-rich SEI, the inorganic lithium

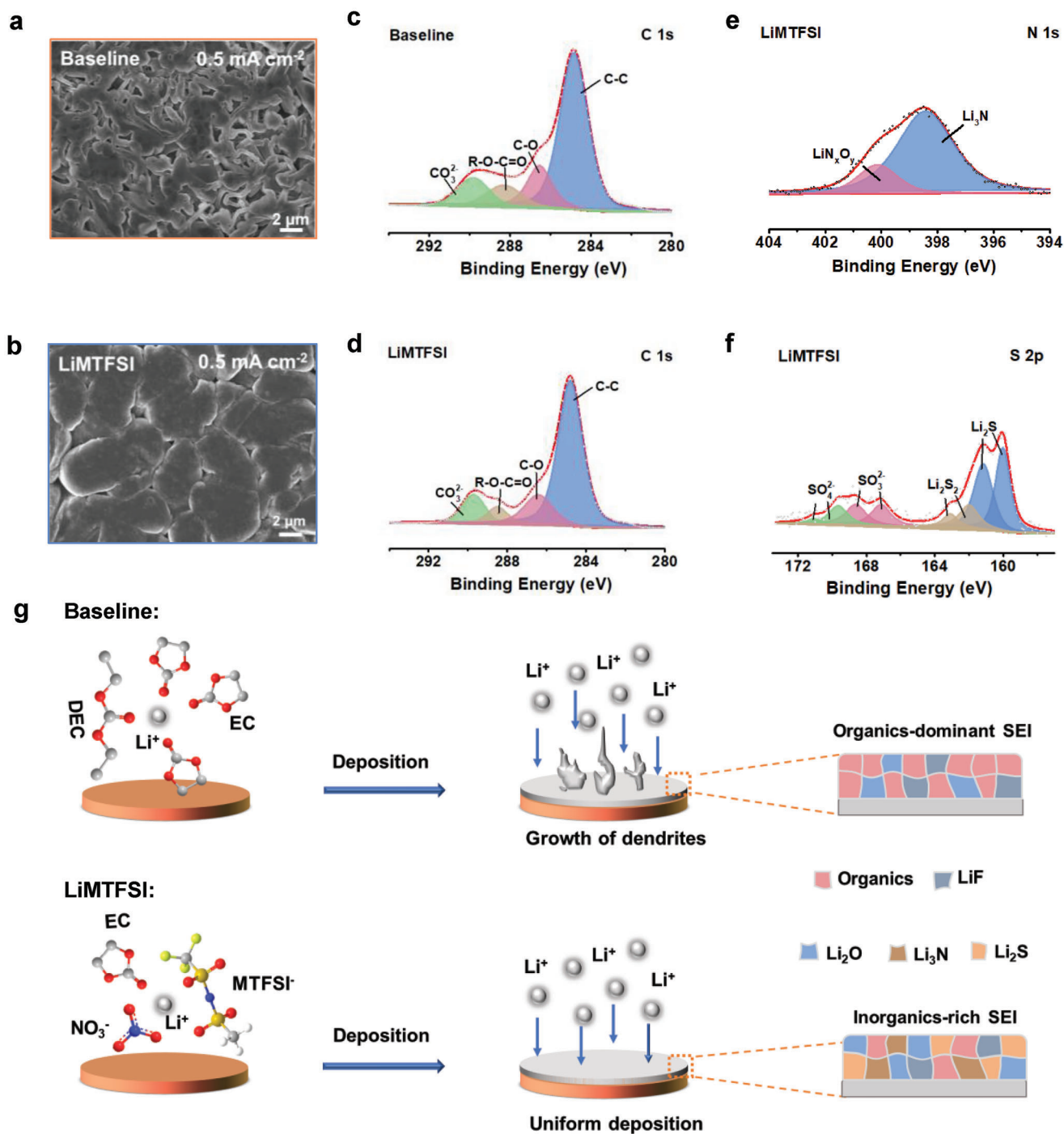


Figure 4. SEM images of deposited Li in a) baseline and b) LiMTFSI electrolytes at 0.5 mA cm^{-2} . c) C 1s XPS spectra of the SEI formed in the c) baseline and d) LiMTFSI electrolytes. e) N 1s and f) S 2p spectra of the SEI formed in the LiMTFSI electrolyte. g) Schematics of the SEI formation process in the baseline electrolyte and LiMTFSI electrolytes.

salts are more chemically stable and possess a lower Li^+ diffusion barrier and higher mechanical strength to withstand the strain produced by lithium dendrites,^[3b,6a] which favors the reversible Li plating/stripping process.

With the enhanced Coulombic efficiency of the Li anode, the electrochemical performance of the Li||NCM523 full cell was in-

vestigated using $40 \mu\text{m}$ thin Li foil as the anode. As shown in **Figure 6a**, the cell with the baseline electrolyte experiences faster capacity decay in the initial stage, retaining only a specific capacity of 117.4 mAh g^{-1} after 150 cycles at 0.5 C, which corresponds to 74.9% of the initial specific capacity. In contrast, the cell with the LiMTFSI electrolyte operates smoothly with an

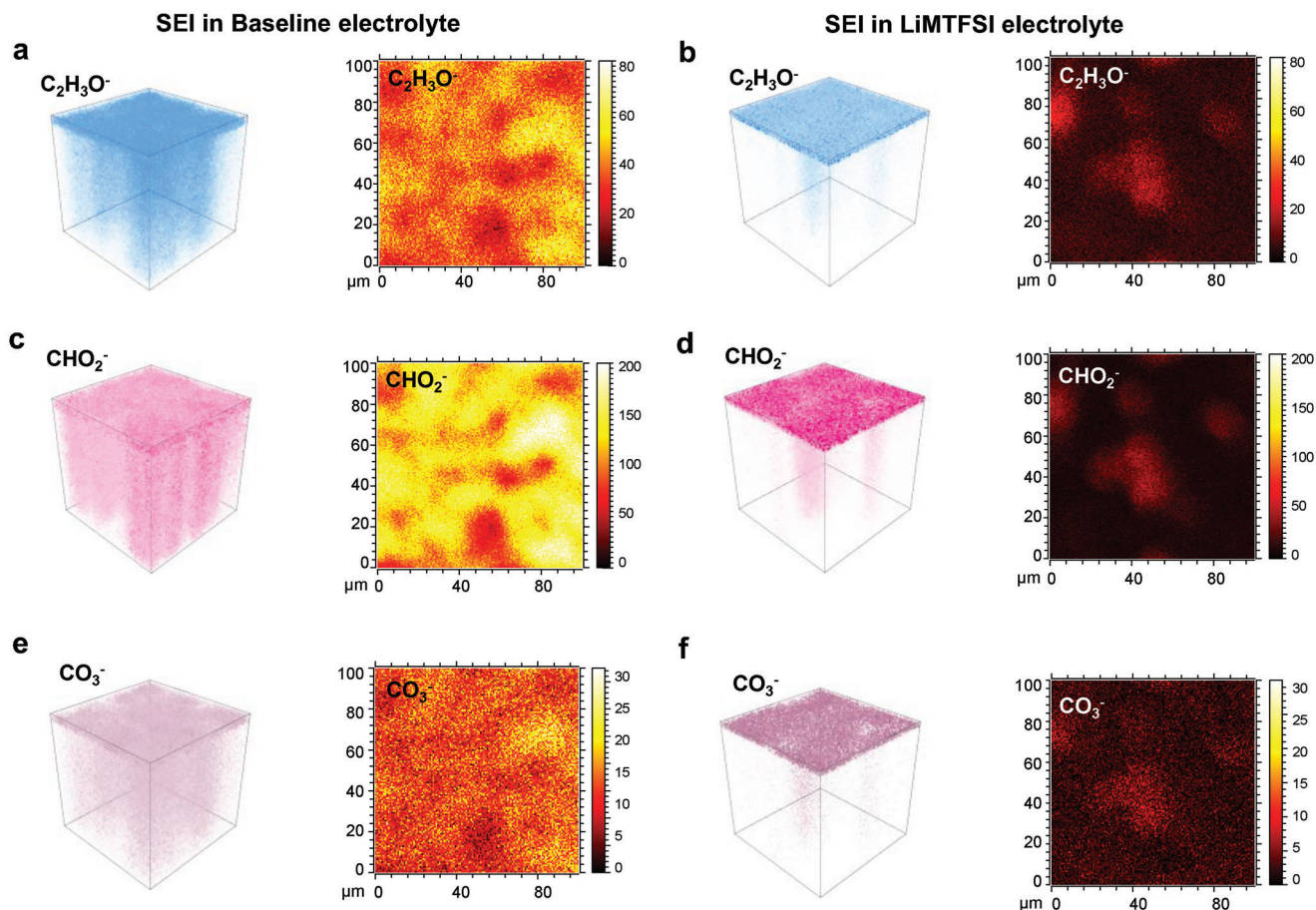


Figure 5. The 3D view (left) and top-view (right) of $C_2H_3O^-$ species in the TOF-SIMS sputtered volumes of the SEI formed in the a) baseline and b) LiMTFSI electrolytes. The 3D view (left) and top view (right) of CHO_2^- species in the TOF-SIMS sputtered volumes of the SEI formed in the c) baseline and d) LiMTFSI electrolytes. The 3D view (left) and top view (right) of CO_3^- species in the TOF-SIMS sputtered volumes of the SEI formed in the e) baseline and f) LiMTFSI electrolytes.

average Coulombic efficiency of 99.5%. After 150 cycles, a specific capacity of 135.5 mAh g^{-1} was still preserved, corresponding to 88.4% of the initial specific capacity, which demonstrates the superiority of LiMTFSI electrolyte at the full-cell level. To simulate more practical conditions, a 500 mAh Li||NCM523 pouch cell was utilized to test the performance of LiMTFSI electrolyte on a larger scale (Figure 6b). As shown in Figure 6c, the two cells with either baseline or LiMTFSI electrolyte exhibit similar capacities in the first few cycles. The time–voltage curve (Figure 6d) demonstrates that the cell with the baseline electrolyte undergoes an over-discharge process after 68 cycles, possibly due to short-circuiting caused by lithium dendrites. With the LiMTFSI electrolyte, however, the CE for Li plating/stripping increased and fewer lithium dendrites appeared. As a result, the cell with LiMTFSI electrolyte operates steadily and maintains a capacity retention of 87.3% after 150 cycles, demonstrating the superior performance of the LiMTFSI electrolyte.

3. Conclusion

Unlike the conventional approach of designing anions with a highly delocalized negative charge, MTFSI[−] anion was specifi-

cally devised by replacing the electron-withdrawing $-CF_3$ group on one side of TFSI[−] with an electron-donating $-CH_3$ group. This modification appropriately reinforces the interaction between Li^+ and the anion, aiming to create more anions in the Li^+ solvation shell. This alteration helps to repel carbonate molecules in the Li^+ solvation sheath and mitigate their reductive decomposition. Consequently, an inorganics-rich SEI comprised of Li_2S , and Li_3N is formed, which suppresses lithium dendrites and enhances the Coulombic efficiency for Li deposition. Moreover, the LiMTFSI-based electrolyte was shown to enable a practical 500 mAh Li||NCM523 pouch cell to run stably for over 150 cycles. We believe this work provides a new perspective for designing advanced lithium salts and suggests that more potential functions of anions could be explored beyond serving as charge carriers in the future.^[15]

4. Experimental Section

Materials Preparations: Trifluoromethanesulfonyl chloride, methanesulfonamide, potassium carbonate (K_2CO_3), pyridine (Py), N, N-dimethylacetamide (DMAC), 1,2-dimethoxyethane (DME), anhydrous acetonitrile, and dichloromethane were purchased from InnoChem

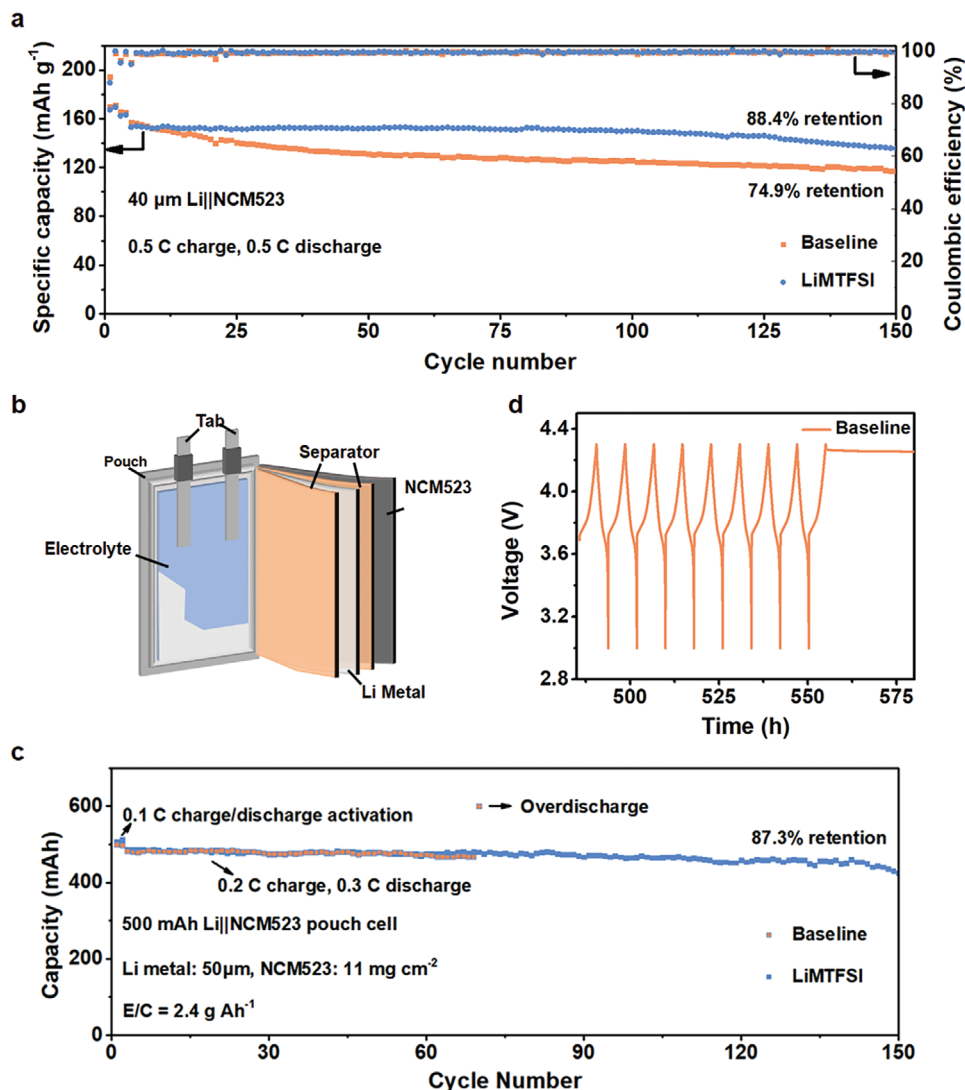


Figure 6. a) Cycling performance of Li||NCM523 coin cells with the baseline and LiMTFSI electrolytes. b) Schematic of a 500 mAh Li||NCM523 pouch cell. c) Cycling performance of 500 mAh Li||NCM523 pouch cells with the baseline and LiMTFSI electrolytes. d) Selected time-voltage profile of the pouch cell with baseline electrolyte.

Technology. Battery-grade lithium bis(trifluoromethanesulfonyl)imide (LiTFSI), sodium bis(trifluoromethanesulfonyl)imide (NaTFSI), lithium hexafluorophosphate (LiPF₆), lithium tetrafluoroborate (LiBF₄), ethylene carbonate (EC), fluoroethylene carbonate (FEC), and diethyl carbonate (DEC) were purchased from DoDoChem. LiNi_{0.5}Co_{0.2}Mn_{0.3}O₂ (NCM523) particles, poly(vinylidene fluoride) (PVDF), super P carbon black, and N-Methylpyrrolidone (NMP) were purchased from Nanjing Mojiesi Energy Technology. 2032-type coin cells and Celgard 2325 separator (25 μm) were purchased from Guangdong Canrd New Energy.

Synthesis of LiMTFSI: Lithium (methanesulfonyl)(trifluoromethanesulfonyl) imide (LiMTFSI) was synthesized in two steps. First, trifluoromethanesulfonyl chloride and methanesulfonamide reacted in the presence of K₂CO₃ in anhydrous acetonitrile, and then potassium (methanesulfonyl)(trifluoromethanesulfonyl) imide (KMTFSI) power was obtained by rotary evaporation of the filtrate. Second, KMTFSI undergoes an ion exchange reaction with LiBF₄ in anhydrous acetonitrile. LiMTFSI was then obtained by rotary evaporation of the filtrate and purified by recrystallization process in anhydrous acetonitrile and dichloromethane.

Electrolytes and Electrode Preparations: The baseline electrolyte was prepared by dissolving 152 mg LiPF₆ in 0.9 mL EC/DEC (1:1 by vol) and 100 μL FEC. The LiMTFSI electrolyte was obtained by adding 23.3 mg LiMTFSI and 6.9 mg LiNO₃ to the baseline electrolyte. More specifically, LiNO₃ and LiMTFSI were first dissolved in EC/DEC and then stirred until being completely dissolved. Then, 152 mg LiPF₆ was dissolved in the prepared solution. The electrolytes were prepared in an argon-filled glove box. To prepare the NCM523 electrode, NCM523 power, poly(vinylidene fluoride) (PVDF), and conductive super P were first mixed in N-methyl pyrrolidone (NMP) with a mass ratio of 90:5:5 to form a slurry. Then, the slurry was coated on a carbon-coated aluminum collector and dried at 100 °C overnight in a vacuum oven. The dried electrodes were then punched into disks with a diameter of 12 mm for cell assembly.

Material Characterizations: Nuclear magnetic resonance (NMR) spectra were recorded on a Bruker Avance III HD 400 or JEOL ECS-400 NMR spectrometer. The diffusion coefficient of Li⁺ and anions was measured by a diffusion-ordered spectroscopy (DOSY). The DN value of EC/DEC solvent and that with LiTFSI or LiMTFSI was determined by ²³Na NMR technique. More specifically, 0.1 M NaTFSI was dissolved in a series of

solvents (including FEC, DME, DMSO, DMAC, DMSO, and Py) with already-known DN, and then the chemical shift of ^{23}Na was measured. Consequently, a fitted linear line relationship was obtained between ^{23}Na chemical shift and the already-known DN of solvents. Then, the DN of pure EC/DEC, LiTFSI-EC/DEC, and LiMTFSI EC/DEC were calculated according to the measured ^{23}Na chemical shift. Raman spectra were obtained by the HORIBA LabRAM HR Evolution Raman system with an excitation laser of 532 nm. The XPS spectra of the SEI were obtained on a Thermo Fisher Scientific ESCALAB Xi. Time-of-flight secondary ion mass spectrometry (TOF-SIMS) spectra and ion images were collected using a Bi^{3+} ion beam accelerated at 30 keV and Cs^+ accelerated at 1 keV. The analyzing area was $100\ \mu\text{m} \times 100\ \mu\text{m}$. The morphology of deposited Li was observed by scanning electron microscope (SEM, JEOL, JSM-7401F, Japan). For XPS and SEM tests, Li metal was first deposited on the Cu substrate and then the Cu substrate was rinsed with DEC to remove residues. Later, it was transferred to a vacuum environment to facilitate solvent evaporation. The XPS and Raman data were analyzed with the XPSPEAK software.

Electrochemical Measurements: All the 2032-type cells were assembled in an argon-filled glove box ($\text{O}_2 < 0.1\ \text{ppm}$, $\text{H}_2\text{O} < 0.1\ \text{ppm}$). The CE of Li plating/stripping was determined by Aurbach's method.^[12] Specifically, 5 mAh cm^{-2} of Li was first deposited on Cu and then charged to the cut-off voltage of 1 V at 0.5 mA cm^{-2} . Following it, 5 mAh cm^{-2} Li was deposited back as a reservoir, followed by a continuous stripping/plating process at 0.5 mA cm^{-2} and 1 mAh cm^{-2} for ten cycles. Finally, the cell was charged to the cut-off voltage. The average CE could be calculated by Equation (1)

$$CE = \frac{10 + Q}{15} \quad (1)$$

where Q is the value of the remaining areal capacity in the final procedure. Electrochemical impedance spectroscopy (EIS) was conducted on a CHI 760E workstation to measure the cell resistance of stainless steel||stainless steel cell and Li||Li symmetric cell from the frequency of 100 kHz to 1 Hz. The conductivity (σ) of the electrolytes in the presence of a separator was calculated according to Equation (2)

$$\sigma = \frac{l}{R \cdot S} \quad (2)$$

where R is the resistance, l is the thickness of the separator, and S is the area of the stainless steel.

The Li^+ transference number was determined by Bruce–Vincent method.^[16] Specifically, a small constant voltage (ΔV) of 5 mV was applied to the Li||Li symmetric cell to detect the initial current (I_{ini}) and the steady-state (I_{ss}) current. The initial (R_{ini}) and steady-state (R_{ss}) interfacial resistances were measured by electrochemical impedance spectroscopy (EIS) over a frequency range from 100 kHz to 1 Hz. Finally, the Li^+ transference number can then be calculated by Equation (3):

$$T_+ = \frac{I_{\text{ss}} * (\Delta V - I_{\text{ini}} * R_{\text{ini}})}{I_{\text{ini}} * (\Delta V - I_{\text{ss}} * R_{\text{ss}})} \quad (3)$$

The Tafel curve was obtained by scanning the Li||Li cell from -0.2 to $0.2\ \text{V}$ with a scanning rate of $0.5\ \text{mV s}^{-1}$. The Li||NCM523 full cells were cycled within the voltage range of 3–4.3 V. The cells were first cycled two times at 0.1 C and 0.25 C for activation, respectively, and then cycled at 0.5 C for charging/discharging. For 500 mAh Li||NCM523 pouch cell, it was first activated at 0.1 C for two cycles, and then charged at 0.2 C and discharged at 0.3 C for cycling.

Supporting Information

Supporting Information is available from the Wiley Online Library or from the author.

Acknowledgements

The author gratefully acknowledges support by the National Key Research and Development Program (2023YFB2503700), the Tsinghua University-China Petrochemical Corporation Joint Institute for Green Chemical Engineering (224247), the National Science Foundation of China (22071133), Beijing Municipal Science & Technology Commission No.Z231100006123003.

Conflict of Interest

The authors declare no conflict of interest.

Data Availability Statement

The data that support the findings of this study are available from the corresponding author upon reasonable request.

Keywords

lithium metal batteries, lithium salt, nucleophilicity, solid electrolyte interphase, solvation sheath

Received: September 9, 2024

Revised: October 2, 2024

Published online:

- a) W. Xu, J. Wang, F. Ding, X. Chen, E. Nasybulin, Y. Zhang, J. G. Zhang, *Energy Environ. Sci.* **2014**, *7*, 513; b) D. Lin, Y. Liu, Y. Cui, *Nat. Nanotechnol.* **2017**, *12*, 194.
- a) K. Xu, *Chem. Rev.* **2014**, *114*, 11503; b) K. Xu, *Chem. Rev.* **2004**, *104*, 4303; c) J. G. Zhang, W. Xu, J. Xiao, X. Cao, J. Liu, *Chem. Rev.* **2020**, *120*, 13312.
- a) X. B. Cheng, R. Zhang, C. Z. Zhao, Q. Zhang, *Chem. Rev.* **2017**, *117*, 10403; b) O. B. Chae, B. L. Lucht, *Adv. Energy Mater.* **2023**, *13*, 2203791.
- a) Z. Zhang, Y. Li, R. Xu, W. Zhou, Y. Li, S. T. Oyakhire, Y. Wu, J. Xu, H. Wang, Z. Yu, D. T. Boyle, W. Huang, Y. Ye, H. Chen, J. Wan, Z. Bao, W. Chiu, Y. Cui, *Science* **2022**, *375*, 66; b) G. M. Hobold, B. M. Gallant, *ACS Energy Lett.* **2022**, *7*, 3458.
- a) Y. Yamada, J. Wang, S. Ko, E. Watanabe, A. Yamada, *Nat. Energy* **2019**, *4*, 269; b) N. Yao, S. Y. Sun, X. Chen, X. Q. Zhang, X. Shen, Z. H. Fu, R. Zhang, Q. Zhang, *Angew. Chem., Int. Ed.* **2022**, *61*, 202210859.
- a) S. Liu, X. Ji, N. Piao, J. Chen, N. Eidson, J. Xu, P. Wang, L. Chen, J. Zhang, T. Deng, S. Hou, T. Jin, H. Wan, J. Li, J. Tu, C. Wang, *Angew. Chem., Int. Ed.* **2021**, *60*, 3661; b) Z. Piao, P. Xiao, R. Luo, J. Ma, R. Gao, C. Li, J. Tan, K. Yu, G. Zhou, H. M. Cheng, *Adv. Mater.* **2022**, *34*, 2108400; c) Y. Jie, X. Liu, Z. Lei, S. Wang, Y. Chen, F. Huang, R. Cao, G. Zhang, S. Jiao, *Angew. Chem., Int. Ed.* **2020**, *59*, 3505; d) N. Piao, S. Liu, B. Zhang, X. Ji, X. Fan, L. Wang, P.-F. Wang, T. Jin, S. C. Liou, H. Yang, J. Jiang, K. Xu, M. A. Schroeder, X. He, C. Wang, *ACS Energy Lett.* **2021**, *6*, 1839.
- a) Z. Wu, R. Li, S. Zhang, L. Lv, T. Deng, H. Zhang, R. Zhang, J. Liu, S. Ding, L. Fan, L. Chen, X. Fan, *Chem* **2023**, *9*, 650; b) X. Ren, S. Chen, H. Lee, D. Mei, M. H. Engelhard, S. D. Burton, W. Zhao, J. Zheng, Q. Li, M. S. Ding, M. Schroeder, J. Alvarado, K. Xu, Y. S. Meng, J. Liu, J. G. Zhang, W. Xu, *Chem* **2018**, *4*, 1877; c) Y. Zhao, T. Zhou, L. P. H. Jeurgens, X. Kong, J. W. Choi, A. Coskun, *Chem* **2023**, *9*, 682; d) Z. Zeng, V. Murugesan, K. S. Han, X. Jiang, Y. Cao, L. Xiao, X. Ai, H. Yang, J. G. Zhang, M. L. Sushko, J. Liu, *Nat. Energy* **2018**, *3*, 674;

- e) L. Suo, Y. S. Hu, H. Li, M. Armand, L. Chen, *Nat. Commun.* **2013**, *4*, 1481; f) S. Jiao, X. Ren, R. Cao, M. H. Engelhard, Y. Liu, D. Hu, D. Mei, J. Zheng, W. Zhao, Q. Li, N. Liu, B. D. Adams, C. Ma, J. Liu, J. G. Zhang, W. Xu, *Nat. Energy* **2018**, *3*, 739; g) X. Fan, X. Ji, L. Chen, J. Chen, T. Deng, F. Han, J. Yue, N. Piao, R. Wang, X. Zhou, X. Xiao, L. Chen, C. Wang, *Nat. Energy* **2019**, *4*, 882; h) X. Dong, Y. Lin, P. Li, Y. Ma, J. Huang, D. Bin, Y. Wang, Y. Qi, Y. Xia, *Angew. Chem., Int. Ed.* **2019**, *58*, 5623.
- [8] a) H. Zhang, Z. Zeng, F. Ma, Q. Wu, X. Wang, S. Cheng, J. Xie, *Angew. Chem., Int. Ed.* **2023**, *62*, 202300771; b) S. Kim, J. A. Lee, T. K. Lee, K. Baek, J. Kim, B. Kim, J. H. Byun, H. W. Lee, S. J. Kang, J. A. Choi, S. Y. Lee, M. H. Choi, J. H. Lee, N. S. Choi, *Energy Environ. Sci.* **2023**, *16*, 5108; c) T. Ma, Y. Ni, Q. Wang, W. Zhang, S. Jin, S. Zheng, X. Yang, Y. Hou, Z. Tao, J. Chen, *Angew. Chem., Int. Ed.* **2022**, *61*, 202207927; d) Y. X. Yao, X. Chen, C. Yan, X. Q. Zhang, W. L. Cai, J. Q. Huang, Q. Zhang, *Angew. Chem., Int. Ed.* **2020**, *60*, 4090; e) Y. Liao, M. Zhou, L. Yuan, K. Huang, D. Wang, Y. Han, J. Meng, Y. Zhang, Z. Li, Y. Huang, *Adv. Energy Mater.* **2023**, *13*, 2301477; f) J. Holoubek, H. Liu, Z. Wu, Y. Yin, X. Xing, G. Cai, S. Yu, H. Zhou, T. A. Pascal, Z. Chen, P. Liu, *Nat. Energy* **2021**, *6*, 303; g) Y. Zhao, T. Zhou, D. Baster, M. El Kazzi, J. W. Choi, A. Coskun, *ACS Energy Lett.* **2023**, *8*, 3180.
- [9] P. Zhou, W. Hou, Y. Xia, Y. Ou, H. Y. Zhou, W. Zhang, Y. Lu, X. Song, F. Liu, Q. Cao, H. Liu, S. Yan, K. Liu, *ACS Nano* **2023**, *17*, 17169.
- [10] a) L. Johnson, C. Li, Z. Liu, Y. Chen, S. A. Freunberger, P. C. Ashok, B. B. Praveen, K. Dholakia, J. M. Tarascon, P. G. Bruce, *Nat. Chem.* **2014**, *6*, 1091; b) V. Gutmann, *Electrochim. Acta* **1976**, *21*, 661; c) R. H. Erlich, A. I. Popov, *J. Am. Chem. Soc.* **2002**, *93*, 5620; d) M. Schmeisser, P. Illner, R. Puchta, A. Zahl, R. van Eldik, *Chem. - Eur. J.* **2012**, *18*, 10969.
- [11] V. Gutmann, E. Wychera, *Inorganic Nuclear Chem. Lett.* **1966**, *2*, 257.
- [12] a) B. D. Adams, J. Zheng, X. Ren, W. Xu, J. G. Zhang, *Adv. Energy Mater.* **2017**, *8*, 1702097; b) D. Aurbach, Y. Gofer, J. Langzam, *J. Electrochem. Soc.* **2019**, *136*, 3198.
- [13] a) T. Ma, Y. Ni, Q. Wang, W. Zhang, S. Jin, S. Zheng, X. Yang, Y. Hou, Z. Tao, J. Chen, *Angew. Chem., Int. Ed.* **2022**, *61*, 202207927; b) F. Cheng, W. Zhang, Q. Li, C. Fang, J. Han, Y. Huang, *ACS Nano* **2023**, *17*, 24259.
- [14] a) S. Ni, M. Zhang, C. Li, R. Gao, J. Sheng, X. Wu, G. Zhou, *Adv. Mater.* **2022**, *35*, 2209028; b) B. Han, Z. Zhang, Y. Zou, K. Xu, G. Xu, H. Wang, H. Meng, Y. Deng, J. Li, M. Gu, *Adv. Mater.* **2021**, *33*, 2100404; c) X. Wu, H. Pan, M. Zhang, H. Zhong, Z. Zhang, W. Li, X. Sun, X. Mu, S. Tang, P. He, H. Zhou, *Adv. Sci.* **2024**, *11*, 2308604.
- [15] a) Y. Xia, P. Zhou, X. Kong, J. Tian, W. Zhang, S. Yan, W. H. Hou, H. Y. Zhou, H. Dong, X. Chen, P. Wang, Z. Xu, L. Wan, B. Wang, K. Liu, *Nat. Energy* **2023**, *8*, 934; b) P. Zhou, H. Zhou, Y. Xia, Q. Feng, X. Kong, W. H. Hou, Y. Ou, X. Song, H. Y. Zhou, W. Zhang, Y. Lu, F. Liu, Q. Cao, H. Liu, S. Yan, K. Liu, *Angew. Chem., Int. Ed.* **2024**, *63*, 202316717.
- [16] P. G. Bruce, C. A. Vincent, *J. Electroanal. Chem.* **1987**, *225*, 1.